Inorganic Chemistry

pubs.acs.org/IC

Article

Room-Temperature Synthesis of $[BMIm][Sn_5O_2Cl_7]$ with $_\infty^1(Sn_2OCl_2)$ Strands in a Saline $[BMIm][SnCl_3]$ Matrix

Silke Wolf, Stefan Seidel, Jens Treptow, Ralf Köppe, Peter W. Roesky, and Claus Feldmann*

Cite This: *Inorg. Chem.* 2022, 61, 4018–4023

Read Online

ACCESS | Metrics & More | Article Recommendations | Supporting Information

ABSTRACT: The novel tin(II) oxychloride $[BMIm][Sn_5O_2Cl_7]$ (BMIm = 1-butyl-3-methylimidazolium) is obtained by the room-temperature reaction (25 °C) of black SnO and $SnCl_2$ in $[BMIm]Cl/SnCl_2$ as an ionic liquid. The title compound can be described as composed of noncharged, infinite $_\infty^1(Sn_2OCl_2)$ strands that are embedded in a saline matrix of $[BMIm]^+$ and $[SnCl_3]^-$. The $_\infty^1(Sn_2OCl_2)$ strands consist of a backbone of edge-sharing $OSn_{4/2}$ tetrahedra, which represent one-dimensional (1D) strands cut out of the layer-type structure of SnO. In $[BMIm][Sn_5O_2Cl_7]$, the $_\infty^1(Sn_2OCl_2)$ strands, which mimic a 1D semiconductor, are terminated by chlorine atoms, whereas they are interconnected by oxygen atoms in the 2D semiconductor SnO. The view of the noncharged $_\infty^1(Sn_2OCl_2)$ strands in a saline $[BMIm][SnCl_3]$ matrix is validated by dissolution experiments. Thus, electron microscopy and Raman spectroscopy show a deconstruction of $[BMIm][Sn_5O_2Cl_7]$ single crystals after treatment with chloroform with a dissolution of $[BMIm][SnCl_3]$, the formation of $SnCl_2$ needles, and tin oxide as a solid remain.

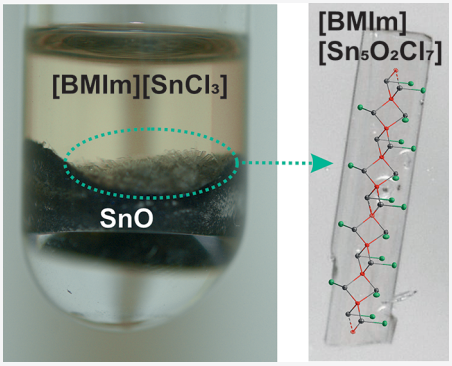

INTRODUCTION

Metal oxides with certain ionic bonding and lattice energy typically require high-temperature solid-state reactions (>400 °C) or polar coordinating solvents to initiate chemical reactions.[1] Thus, either sufficient diffusion in the solid state or the formation of coordination complexes needs to be guaranteed. Synthesis at high temperatures, however, is counterproductive in regard to novel metastable compounds and favors formation of the thermodynamically most stable compounds.[2,3] In liquid-phase reactions, the dissolution of metal oxides requires the formation of coordination complexes with ligands that, thereafter, may significantly influence the composition, bonding, and properties of the obtained compounds. For these reasons, reactions of metal oxides near room temperature (≤100 °C) and in the absence of coordinating solvents/ligands are rare.

Ionic liquids have significantly advanced the synthesis of inorganic compounds near room temperature (≤100 °C), leading to spectacular metastable compounds that would have been impossible to prepare in conventional solvents.[4,5] Selected examples include the polychloride $[Et_4N]_2[(Cl_3)_2 \cdot Cl_2]$,[6] the intermetalloid $[CuBi_8]^{3+}$ cluster cation in $[CuBi_8][AlCl_4]_2[Al_2Cl_7]$,[7] the heavy-metal porphyrin analogue $[Hg_4Te_8(Te_2)_4]^{8-}$ in $[DMIm]_8[Hg_4Te_8(Te_2)_4]$ ($[DMIm]^+$ = 1-decyl-3-methylimidazolium),[8] the ligand-stabilized $[Ga_5]^{5+}$ pentagon,[9] or the linear uranyl-type $[N{\equiv}U{\equiv}N]$ cluster core.[10] As part of our studies, we could add the three-dimensional (3D) polybromide $[C_4MPyr]_2[Br_{20}]$[11] or the highly coordinated $Sn^{II}I_8$ subunit in the carbonyl $[SnI_8\{Fe(CO)_4\}_4][Al_2Cl_7]_2$.[12] Key advantages of ionic liquids comprise their special solvent properties, such as their high thermal and chemical stability and weakly coordinating properties.[4,5,13] The synthesis of metastable compounds in ionic liquids has so far predominately involved metal halides, selenides/tellurides, or metal clusters.[4−12] In comparison, the synthesis of new metal oxides in ionic liquids has been rare until now, which can be ascribed to their aforementioned high lattice energy and their, in comparison to metal halides or metal compounds of the heavier chalcogenides, low solubility in ionic liquids. Meanwhile, several studies have already evaluated the conditions for how to dissolve metal oxides in ionic liquids.[14−16] Syntheses of novel metal oxide compounds are, nevertheless, rare.

Aiming at the synthesis of novel metal oxide compounds via an ionic-liquid-based synthesis, we here describe the novel tin oxychloride $[BMIm][Sn_5O_2Cl_7]$ (BMIm = 1-butyl-3-methylimidazolium), which was obtained by the reaction of black SnO and $SnCl_2$ at room temperature (25 °C) in $[BMIm]Cl/SnCl_2$. The title compound is composed of noncharged, infinite $_\infty^1(Sn_2OCl_2)$ strands that are embedded in a saline matrix of $[BMIm]^+$ cations and $[SnCl_3]^-$ anions. The crystal structure of the title compound and dissolution experiments to

Received: December 3, 2021
Published: February 24, 2022

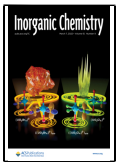

https://doi.org/10.1021/acs.inorgchem.1c03763
Inorg. Chem. 2022, 61, 4018−4023

probe the view of $_{\infty}^{1}(Sn_2OCl_2)$ strands in a saline matrix are described.

EXPERIMENTAL METHODS

General Considerations. All reactions were performed using standard Schlenk techniques or argon-filled gloveboxes (H_2O, O_2 < 0.1 ppm, MBraun Unilab). Commercially available tetragonal, black SnO (99%, ABCR) and $SnCl_2$ (anhydrous, 97%, Acros) were used as supplied. 1-Butyl-3-methylimidazolium chloride ([BMIm]Cl, 99%, Iolitec) was dried at 130 °C for 3 days in a vacuum (10^{-3} mbar) prior to use.

[BMIm][$Sn_5O_2Cl_7$] was prepared by mixing [BMIm]Cl (600.0 mg, 3.4 mmol, 1 equiv) and $SnCl_2$ (1300.8 mg, 6.9 mmol, 2 equiv) in a Schlenk tube at room temperature. The mixture was stirred for a few minutes, which resulted in a yellowish solution. SnO (924.0 mg, 6.9 mmol, 2 equiv) was added to the solution and stirred for 6 h at room temperature. The insoluble black SnO precipitates slowly to the bottom of the Schlenk tube. Within 3 weeks, the growth of colorless, needle-shaped crystals was observed at the interface of the SnO slurry and ionic liquid with an estimated yield of about 20%. This limited yield can be predominately related to the slow reaction.

As an alternative, the synthesis of [BMIm][$Sn_5O_2Cl_7$] can also be performed with slight heating to 40 °C for 3 weeks. In comparison to the aforementioned room-temperature reaction, this results in large transparent single crystals with a size of up to 1 mm. However, colorless plates of [BMIm][Sn_3Cl_7] were also obtained, which was not observed for the room-temperature reaction.

Analytical Techniques. Details of the analytical methods can be obtained from the Supporting Information. Further details of the crystal structure are listed in Table S1 and can also be obtained from the joint CCDC/FIZ Karlsruhe deposition service upon quoting the depository number 2123506.

RESULTS AND DISCUSSION

Synthesis. The novel tin oxychloride [BMIm][$Sn_5O_2Cl_7$] was prepared by the reaction of SnO and $SnCl_2$ in [BMIm]Cl/$SnCl_2$ (1:2 ratio) at room temperature (25 °C) according to the following equation:

$$2SnO + 2SnCl_2 + [BMIm]^+ + [SnCl_3]^- \rightarrow [BMIm][Sn_5O_2Cl_7]$$

At first glance, the reaction can be rationalized as a Lewis acid−base reaction with $SnCl_2$ as the acid and SnO as the base. When considering the low oxidation state and the lone pair of Sn^{II}, however, the reaction and product are actually surprising because $SnCl_2$ is only a weak Lewis acid. Moreover, SnO is also only a weak Lewis base and hardly soluble in the ionic liquid (Figure 1a). Nevertheless, colorless needle-shaped crystals of [BMIm][$Sn_5O_2Cl_7$] grow within 3 weeks at the interface of the black bottom slurry of SnO and the yellowish ionic liquid as the top phase (Figure 1b). Optical spectroscopy confirms the presence of a wide-band-gap material with an absorption below 350 nm ($E_g \sim 3.5$ eV; Figure S1). The crystals are highly stable in the mother liquor and under inert conditions, but they rapidly deliquesce in the presence of moisture.

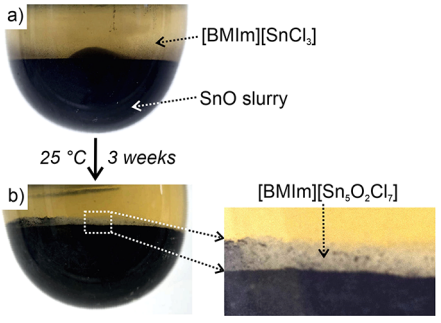

Figure 1. Room-temperature synthesis of [BMIm][$Sn_5O_2Cl_7$]: (a) Dark slurry of SnO with a [BMIm]Cl/$SnCl_2$ (1:2) top phase prior to the reaction. (b) Crystal growth at the interface after 3 weeks.

Structural Characterization. According to single-crystal structure analysis, [BMIm][$Sn_5O_2Cl_7$] crystallizes in the space group $P\bar{1}$ and consists of noncharged, infinite $_{\infty}^{1}(Sn_2OCl_2)$ strands as well as $[BMIm]^+$ cations and $[SnCl_3]^-$ anions (Figure 2 and Table S1). The chemical composition was validated by energy-dispersive X-ray spectroscopy (EDXS) of single crystals, resulting in a Sn/Cl ratio of 41(1):59(1), which is in accordance with expectations (calculated Sn/Cl ratio of 42:58).

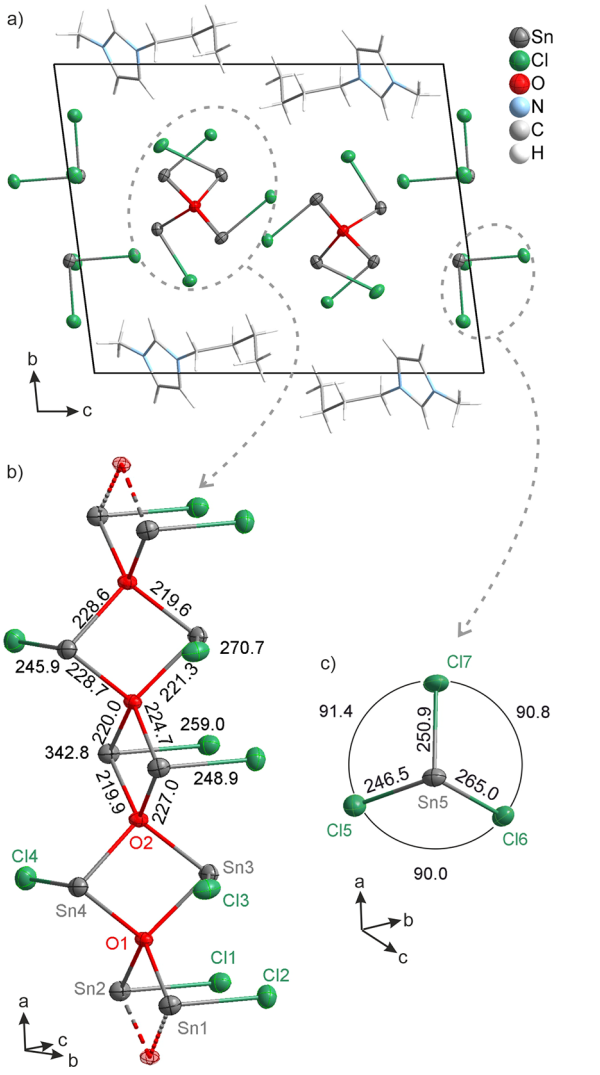

Figure 2. Crystal structure of [BMIm][$Sn_5O_2Cl_7$]: (a) Unit cell in the *bc* plane. (b) $_{\infty}^{1}(Sn_2OCl_2)$ strand with edge-sharing OSn_4 tetrahedra along the *a* axis. (c) $[SnCl_3]^-$ anion (selected distances are in picometers and selected angles in degrees; anisotropic displacement parameters with 50% probability).

The noncharged $_{\infty}^{1}(Sn_2OCl_2)$ strands are established by a backbone of edge-sharing OSn_4 tetrahedra along the crystallographic *a* axis (Figures 2a and S2). All four crystallographically

https://doi.org/10.1021/acs.inorgchem.1c03763
Inorg. Chem. 2022, 61, 4018−4023

independent tin atoms are coordinated by two bridging oxygen atoms and a terminal chlorine atom. Together with the lone pair at the tin(II) atoms, a distorted trigonal ($SnO_{2/4}Cl$) pyramid is formed as the coordination polyhedron (Figure 2b). The Sn−O distances of 219.6(3)−228.7(3) pm are well comparable to those in SnO (221 pm).[17] The Sn−Cl distances are widely spread and range from 245.9(2) to 270.7(2) pm, which is shorter than those in $SnCl_2$ (266.4−305.8 pm;Tables S2 and S3).[18]

The strands of edge-sharing OSn_4 tetrahedra can be considered to be a one-dimensional (1D) cutout of the two-dimensional (2D) layer-type structure of the tetragonal, black modification of SnO (Figure 3).[17] Thus, the $_\infty^1(Sn_2OCl_2)$

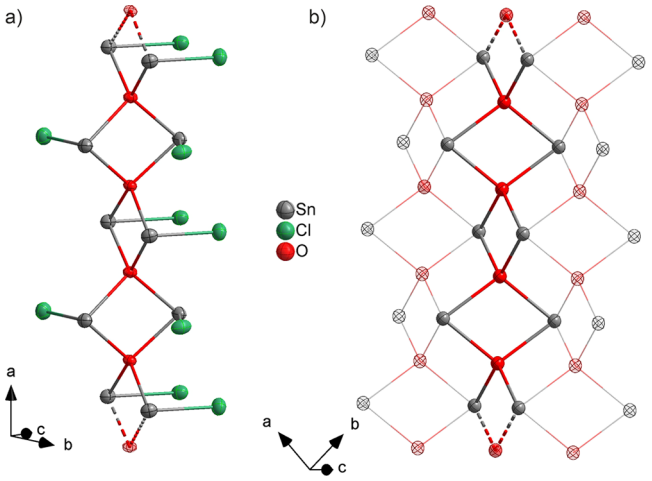

Figure 3. Comparison of the 1D strands $_\infty^1(Sn_2OCl_2)$ in $[BMIm][Sn_5O_2Cl_7]$ with the 2D-layer structure of the tetragonal, black modification of SnO: (a) $_\infty^1(Sn_2OCl_2)$ strand with edge-sharing OSn_4 tetrahedra. (b) SnO layer with one row of edge-sharing OSn_4 tetrahedra highlighted.

strands can also be considered to be 1D semiconducting units cut out of the 2D semiconductor SnO. In comparison to SnO, the Sn−O bonds leading to the 2D arrangement of edge-sharing OSn_4 tetrahedra are terminated by chlorine atoms in $[BMIm][Sn_5O_2Cl_7]$. In contrast, tin oxyhalides such as Sn_2OF_2[19] or Sn_4OF_6[20] exhibit a 3-fold almost planar coordination of the oxygen atoms. A tetrahedral OSn_4 coordination was observed for two of four oxygen atoms in $Sn_7O_4Cl_6$[21] or in the oxyhydroxide $Sn_{21}Cl_{16}(OH)_{14}O_6$.[22] Comparable tetrahedral OPb_4 chains are rather known from lead(II) oxyhalides, such as Pb_2OF_2[23] and $Pb_{17}Cl_{18}O_8$[24] (both with single tetrahedral OPb_4 chains) or $Pb_3O_2Cl_2$.[25] Here, it must be noticed that these compounds are usually prepared by solid-state reactions at elevated temperature (≥200 °C).

Besides the closest Sn−O and Sn−Cl distances in the $_\infty^1(Sn_2OCl_2)$ strand and the $[SnCl_3]^-$ anion, further secondary Sn···Cl interactions (309.3(1)−382.7(2) pm) occur that are shorter than the sum of the van der Waals radii (Sn−Cl = 395 pm)[26] and, thus, contribute to the overall bonding situation (Tables S2 and S3). Together with these secondary interactions, a 3 + 4 (Sn1 and Sn4), 3 + 5 (Sn2 and Sn3), and 3 + 3 (Sn5) coordination is obtained (Figure S3). Secondary Sn···Cl interactions also lead to an interconnection of the $_\infty^1(Sn_2OCl_2)$ strands and $[SnCl_3]^-$ anions (Figure S4), resulting in $_\infty^2[Sn_5O_2Cl_7]^-$ layers, which are separated by the $[BMIm]^+$ cations. These Sn···Cl distances are in good agreement with secondary Sn···Cl interactions in $SnCl_2$ (321.9−330.2 pm),[18] which are typically considered to be up to a limit of 360 pm (Tables S2 and S3).[27]

The $[BMIm]^+$ cations and $[SnCl_3]^-$ anions exhibit as-expected distances. Similar to the $_\infty^1(Sn_2OCl_2)$ strands, the $[SnCl_3]^-$ anions have a distorted pyramidal coordination including the stereochemically active lone pair (Figure 2c). The Sn−Cl distances (246.5(2)−265.0(2) pm) are again in good agreement with the literature (e.g., $Cs[SnCl_3]$ with 250−255 pm; Tables S2 and S3).[28] The Cl−Sn−Cl angles (90.0(1)−91.4(1)°) are as well in accordance with the literature (e.g., $Cs[SnCl_3]$ with 86.9−92.3°)[28] and indicate the sterical influence of the aforementioned secondary Sn···Cl interactions. Furthermore, hydrogen bridging is observed between $[SnCl_3]^-$ and $[BMIm]^+$ with Sn−Cl···H−C distances of 274(1)−299(1) pm, which are partly below the sum of the van der Waals radii (295 pm).[26] Finally, it needs to be noticed that the Sn···Sn distances in the $_\infty^1(Sn_2OCl_2)$ strands (339−343 pm) are even shorter than those in SnO (351 pm)[17] and not far from the Sn−Sn distances in the metal (302−318 pm).[29]

Dissolution Studies. To verify the view of the $_\infty^1(Sn_2OCl_2)$ strands in a saline $[BMIm][SnCl_3]$ matrix, dissolution experiments were performed in order to probe an optional separation of the weakly bound voluminous $[BMIm]^+/[SnCl_3]^-$ ions and the stronger bound $_\infty^1(Sn_2OCl_2)$ strands (Figure 4a). To this concern, single

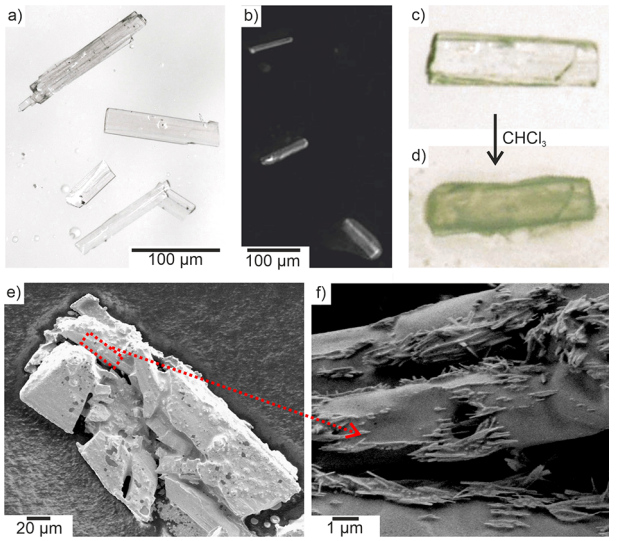

Figure 4. Treatment of single crystals of $[BMIm][Sn_5O_2Cl_7]$. (a−c) Light microscopy and SEM images of the as-prepared single crystals. (d−f) Light microscopy and SEM/TEM images of the single-crystal remains after $CHCl_3$ treatment at different levels of magnification.

crystals of $[BMIm][Sn_5O_2Cl_7]$ were rinsed with small portions of dry chloroform ($CHCl_3$) at room temperature (25 °C). Already optical, the crystals changed as they became smaller and turned from colorless to light yellowish-brown (Figure 4a,c,d). Scanning electron microscopy (SEM) already confirms disintegration of the single crystals (Figure 4b,e). After the evaporation of all $CHCl_3$, moreover, transmission electron microscopy (TEM) indicates the formation of tiny needles covering the crystal surfaces as well as the formation of a spongy precipitate around the single-crystal remains (Figure 4f).

https://doi.org/10.1021/acs.inorgchem.1c03763
Inorg. Chem. 2022, 61, 4018−4023

To elucidate the underlying dissolution process and to identify the different products, EDXS and Raman microscopy were applied (Figures 5 and 6). Here, it must be noticed that

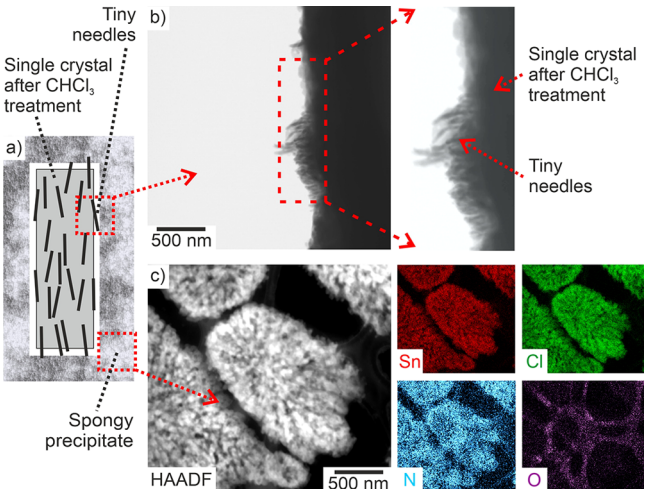

Figure 5. Treatment of a $[BMIm][Sn_5O_2Cl_7]$ single crystal with $CHCl_3$: (a) Scheme of single-crystal remains with tiny needles and a spongy precipitate. (b) TEM image of tiny needles on the surface of single-crystal remains (EDXS performed in the area of the red box; Table 1). (c) TEM image and EDXS area scans of a spongy precipitate around the single-crystal remains (EDXS data shown in Table 1).

EDXS line scans were not successful because of complete destruction under the conditions of high-energy electron bombardment. EDXS area scans, however, reveal the composition of the tiny needles and of the spongy precipitate. Accordingly, EDXS of the tiny crystals resulted in a Sn/Cl ratio of 1:2.2 with only low quantities of oxygen (Table 1 and Figure 5a,b), which points to the formation of $SnCl_2$. For the spongy precipitate around the single crystal, EDXS area scans show N/Sn/Cl with a ratio of 1.8:1:2.9 and again only low quantities of oxygen (Table 1 and Figure 5a,c). This is in agreement with the presence of $[BMIm][SnCl_3]$ (N:Sn:Cl = 2:1:3). As a result, $CHCl_3$ obviously dissolves the saline $[BMIm][SnCl_3]$ matrix out of the $[BMIm][Sn_5O_2Cl_7]$ single crystals. The dissolved $[BMIm][SnCl_3]$ is deposited in the area around the single crystals after the evaporation of $CHCl_3$. Moreover, $SnCl_2$ is formed, which is insoluble in $CHCl_3$ and, thus, crystallizes in the form of tiny needles on the surface of the single-crystal remains.

Table 1. EDXS Data (atom %) of $[BMIm][Sn_5O_2Cl_7]$. Products after $CHCl_3$ Treatment

	elements (atom %)					
	Sn	Cl	C[a]	N	O	Cu[b]
tiny needles	13.0	28.8	51.9[a]	1.2	4.2	0.9[b]
spongy precipitate	4.1	12.1	74.8[a]	7.2	1.1	0.7[b]
	element ratio[c]					
	Sn	Cl	C	N	O	
tiny needles	1	2.2	*a*	0.1	0.3	
spongy precipitate	1	3.0	*a*	1.8	0.2	
$[BMIm][SnCl_3](Sn_2OCl_2)$	5	7	8	2	2	
$[BMIm][SnCl_3]$	1	3	8	2		
$SnCl_2$	1	2				

[a]C cannot be determined because of amorphous carbon (lacey-)film-coated copper grids. [b]Cu originating from amorphous carbon (lacey-)film-coated copper grids. [c]Element ratios calculated based the above EDXS data.

In regard to the solid remaining after the $CHCl_3$ treatment, it must be noticed that EDXS was again not successful because the single-crystal remains were completely destroyed under the conditions of high-energy electron bombardment. This was also caused by the thickness of the insulating sample, which is significantly thicker at the position of the disintegrated single crystal than that for the tiny $SnCl_2$ crystals or the $[BMIm][SnCl_3]$ sponge. Therefore, $[BMIm][Sn_5O_2Cl_7]$ single crystals as well as the single-crystal remains after the $CHCl_3$ treatment were analyzed by Raman spectroscopy (Figures 6 and S5–S7). In addition, Raman spectra were calculated by means of quantum-chemical density functional theory methods (see the Supporting Information for details) based on a $[SnCl_3]^-$ unit as well as an almost linear $[Sn_{18}O_{10}Cl_{18}]^{2-}$ model subunit (with C_s symmetry) of the noncharged $_\infty^1(Sn_2OCl_2)$ strands (Tables S4 and S5 and Figures S8 and S9). On the basis of the calculated spectra (Tables S6 and S7 and Figures S9 and S10), the Raman intensities at 265 and 130 cm^{-1} can be attributed to Sn–Cl stretching and deformation vibrations,[30] whereas the Raman intensities at 210–160 cm^{-1} are related to the Sn–O deformation modes.[31] On the basis of the calculated data, the most intense vibrations of the experimentally observed Raman spectrum of the $[BMIm][Sn_5O_2Cl_7]$ single crystals at 285, 263, and 134 cm^{-1} can be attributed to the formal A_{1g} and E_g stretching motions and the A_{1g} deformation modes of the $[SnCl_3]^-$ unit (with local C_{3v} symmetry).[30] They coincide with the Sn–Cl motions of the $_\infty^1(Sn_2OCl_2)$ strands, whereas the Sn–O vibrations are peaking at 208 cm^{-1} (Figure 6c).

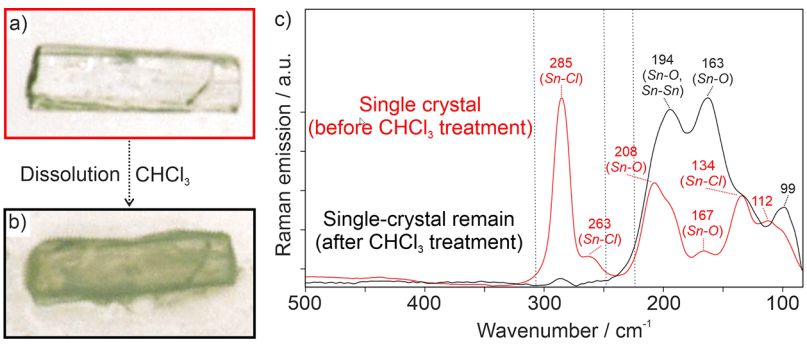

Figure 6. $[BMIm][Sn_5O_2Cl_7]$ single crystal before and after treatment with $CHCl_3$: (a and b) Scheme of a single crystal. (c) Raman spectra of a single crystal (Figures S5–S7).

https://doi.org/10.1021/acs.inorgchem.1c03763
Inorg. Chem. 2022, 61, 4018–4023

After the $CHCl_3$ treatment, Raman signals of the Sn−Cl vibrations as well as those originating from $[BMIm]^+$ vanish almost completely for the single-crystal remains, whereas those of the Sn−O vibrations are still present and now appear with higher intensity (Figures 6c and S5−S7). For the Sn−O vibrations, moreover, a significant broadening and a certain shift to lower wavenumbers (maxima at 194 and 163 cm^{-1}) are indicative. These findings point to the formation of a binary tin oxide with a stoichiometry between SnO (Raman bands expected at 210 and 115 cm^{-1})[32] and SnO_2 (Raman bands expected at 480, 639, and 782 cm^{-1})[33] and, thus, to Sn_2O_3[33] or Sn_3O_4.[34] After removal of the saline matrix from $[BMIm][Sn_5O_2Cl_7]$, such decomposition can be ascribed to the structural instability of the remaining tin(II) oxide strands, which triggers a disproportionation to tin(0) and tin(IV) rather than to tin(III).[35,36] Furthermore, experimental indication for the appearance of tin(0) is given by the Raman band at 194 cm^{-1}, which is in accordance with not only a Sn−O vibration but also the Raman spectrum of α-Sn.[37] In summary, EDXS and Raman spectroscopy point to dissolution of the saline $[BMIm][SnCl_3]$ matrix of $[BMIm][Sn_5O_2Cl_7]$, the formation of $SnCl_2$, and tin oxide as a solid remain. The latter further disproportionates to Sn_3O_4 and Sn.

CONCLUSIONS

$[BMIm][Sn_5O_2Cl_7]$ (BMIm = 1-butyl-3-methylimidazolium) was obtained as a novel tin(II) oxychloride by the room-temperature reaction (25 °C) of SnO and $SnCl_2$ in $[BMIm]Cl/SnCl_2$ as an ionic liquid. Besides the low temperature as such, this Lewis acid−base reaction of $SnCl_2$ and SnO is surprising because both $SnCl_2$ and SnO are only a weak Lewis acid and base. SnO as a barely soluble solid, nevertheless, reacts to $[BMIm][Sn_5O_2Cl_7]$ with colorless needle-shaped crystals that grow within 3 weeks at the interface between the black bottom slurry of SnO and the yellowish ionic liquid as the top phase. According to single-crystal structure analysis, the composition of the title compound can be described to consist of noncharged, infinite $_\infty^1(Sn_2OCl_2)$ strands, which are embedded in a saline matrix of $[BMIm]^+$ and $[SnCl_3]^-$. The $_\infty^1(Sn_2OCl_2)$ backbone of edge-sharing $OSn_{4/2}$ tetrahedra is unusual for tin oxides and tin oxyhalides. It represents a 1D cutout of the layer-type structure of the 2D semiconductor SnO and can be considered to mimic a 1D semiconductor. The view of the noncharged $_\infty^1(Sn_2OCl_2)$ strands in a saline $[BMIm][SnCl_3]$ matrix is validated by dissolution experiments. Accordingly, electron microscopy (SEM and TEM), electron spectroscopy (EDXS), and Raman spectroscopy point to a deconstruction of $[BMIm][Sn_5O_2Cl_7]$ single crystals upon treatment with $CHCl_3$ with a dissolution of $[BMIm][SnCl_3]$, the formation of $SnCl_2$ needles, and tin oxide as a solid remain. The room-temperature reaction and novel compound point to the advantage of ionic liquids and exemplarily show the option to prepare novel metal oxide compounds near room temperature (≤100 °C) and in the absence of coordinating solvents/ligands. In principle, such a synthesis strategy could allow one to realize much more metastable metal oxides, which are not accessible by high-temperature syntheses or conventional solvent-based reactions.

ASSOCIATED CONTENT

Supporting Information

The Supporting Information is available free of charge at https://pubs.acs.org/doi/10.1021/acs.inorgchem.1c03763.

Details related to the analytical techniques, structure analysis, Raman spectroscopy, and quantum-chemical calculations (PDF)

Accession Codes

CCDC 2123506 contains the supplementary crystallographic data for this paper. These data can be obtained free of charge via www.ccdc.cam.ac.uk/data_request/cif, or by emailing data_request@ccdc.cam.ac.uk, or by contacting The Cambridge Crystallographic Data Centre, 12 Union Road, Cambridge CB2 1EZ, UK; fax: +44 1223 336033.

AUTHOR INFORMATION

Corresponding Author

Claus Feldmann − *Institute for Inorganic Chemistry, Karlsruhe Institute of Technology, D-76131 Karlsruhe, Germany*; orcid.org/0000-0003-2426-9461; Email: claus.feldmann@kit.edu

Authors

Silke Wolf − *Institute for Inorganic Chemistry, Karlsruhe Institute of Technology, D-76131 Karlsruhe, Germany*

Stefan Seidel − *Institute for Inorganic and Analytical Chemistry, University of Münster, D-48149 Münster, Germany*

Jens Treptow − *Institute for Inorganic Chemistry, Karlsruhe Institute of Technology, D-76131 Karlsruhe, Germany*

Ralf Köppe − *Institute for Inorganic Chemistry, Karlsruhe Institute of Technology, D-76131 Karlsruhe, Germany*; orcid.org/0000-0002-0492-0803

Peter W. Roesky − *Institute for Inorganic Chemistry, Karlsruhe Institute of Technology, D-76131 Karlsruhe, Germany*; orcid.org/0000-0002-0915-3893

Complete contact information is available at: https://pubs.acs.org/10.1021/acs.inorgchem.1c03763

Notes

The authors declare no competing financial interest.

ACKNOWLEDGMENTS

The authors thank the Deutsche Forschungsgemeinschaft (DFG) for funding in the Priority Program SPP1708 ("Material synthesis near room temperature"). The authors also acknowledge computational support by the state of Baden-Württemberg through bwHPC and the DFG through Grant INST 40/467-1 FUGG.

REFERENCES

(1) West, A. R. *Solid State Chemistry and Its Applications*, 2nd ed.; Wiley: Chichester, U.K., 2014.

(2) Jansen, M.; Schon, J. C. Structure Prediction in Solid-State Chemistry as an Approach to Rational Synthesis Planning. In *Comprehensive Inorganic Chemistry II*; Reedijk, J., Poeppelmeier, K., Eds.; Elsevier: New York, 2013; Vol. *9*, pp 941−969.

(3) Feldmann, C. Metastable Solids − Terra Incognita Awaiting Discovery. *Angew. Chem., Int. Ed.* **2013**, *52*, 7610−7611.

(4) Zhang, T.; Doert, T.; Wang, H.; Zhang, S.; Ruck, M. Inorganic Synthesis Based on Reactions of Ionic Liquids and Deep Eutectic Solvents. *Angew. Chem. Int. Ed. 2021, Angew. Chem. Int. Ed.* **2021**, *60*, 22148−22165.

(5) Freudenmann, D.; Wolf, S.; Wolff, M.; Feldmann, C. Ionic Liquids – New Perspectives for Inorganic Synthesis Chemistry? *Angew. Chem., Int. Ed.* **2011**, *50*, 11050–11060.
(6) Brueckner, R.; Haller, H.; Steinhauer, S.; Mueller, C.; Riedel, S. A 2D Polychloride Network Held Together by Halogen-Halogen Interactions. *Angew. Chem., Int. Ed.* **2015**, *54*, 15579–15583.
(7) Knies, M.; Kaiser, M.; Isaeva, A.; Mueller, U.; Doert, T.; Ruck, M. The Intermetalloid Cluster Cation $(CuBi_8)^{3+}$. *Chem. Eur. J.* **2018**, *24*, 127–132.
(8) Donsbach, C.; Reiter, K.; Sundholm, D.; Weigend, F.; Dehnen, S. $[Hg_4Te_8(Te_2)_4]^{8-}$: A Heavy Metal Porphyrinoid Embedded in a Lamellar Structure. *Angew. Chem., Int. Ed.* **2018**, *57*, 8770–8774.
(9) Glootz, K.; Himmel, D.; Kratzert, D.; Butschke, B.; Scherer, H.; Krossing, I. Why Do Five Ga^+ Cations Form a Ligand-Stabilized $[Ga_5]^{5+}$ Pentagon and How Does a 5:1 Salt Pack in the Solid State? *Angew. Chem., Int. Ed.* **2019**, *58*, 14162–14166.
(10) Rudel, S. S.; Deubner, H. L.; Mueller, M.; Karttunen, A. J.; Kraus, F. Complexes featuring a linear $[N{\equiv}U{\equiv}N]$ core isoelectronic to the uranyl cation. *Nat. Chem.* **2020**, *12*, 962–967.
(11) Wolff, M.; Meyer, J.; Feldmann, C. $[C_4MPyr]_2[Br_{20}]$ – Ionic Liquid based Synthesis of the first three-dimensional Polybromide Network. *Angew. Chem., Int. Ed.* **2011**, *50*, 4970–4973.
(12) Wolf, S.; Köppe, R.; Block, T.; Pöttgen, R.; Roesky, P. W.; Feldmann, C. $SnI_8\{Fe(CO)_4\}_4]^{2+}$: Highly-coordinated $Sn^{+II}I_8$ Subunit with Fragile Carbonyl Clips. *Angew. Chem., Int. Ed.* **2020**, *59*, 5510–5514.
(13) Wasserscheid, P.; Welton, T. *Ionic Liquids in Synthesis*; Wiley-VCH: Weinheim, Germany, 2008.
(14) Nockemann, P.; Thijs, B.; Parac-Vogt, T. N.; Van Hecke, K.; Van Meervelt, L.; Tinant, B.; Hartenbach, I.; Schleid, T.; Ngan, V. T.; Nguyen, M. T.; Binnemans, K. Carboxyl-Functionalized Task-Specific Ionic Liquids for Solubilizing Metal Oxides. *Inorg. Chem.* **2008**, *47*, 9987–9999.
(15) Wellens, S.; Brooks, N. R.; Thijs, B.; Van Meervelt, L.; Binnemans, K. Carbene Formation Upon Reactive Dissolution of Metal Oxides in Imidazolium Ionic Liquids. *Dalton Trans.* **2014**, *43*, 3443–3452.
(16) Richter, J.; Ruck, M. Dissolution of Metal Oxides in Task-Specific Ionic Lquid. *RSC Adv.* **2019**, *9*, 29699–29710.
(17) Moore, W. J.; Pauling, L. The Crystal Structures of the Tetragonal Monoxides of Lead, Tin, Palladium, and Platinum. *J. Am. Chem. Soc.* **1941**, *63*, 1392–1394.
(18) van den Berg, J. M. The Crystal Structure of $SnC1_2$. *Acta Crystallogr.* **1961**, *14*, 1002–1003.
(19) Darriet, P. B.; Galy, J. Synthèse et Structure Cristalline du Bis[difluorooxostannate(II)] d'étain(II), $(Sn_2O_2F_4)Sn_2$. *Acta Crystallogr. B* **1977**, *33*, 1489–1492.
(20) Abrahams, I.; Clark, S. J.; Donaldson, J. D.; Khan, Z. I.; Southern, J. T. Hydrolysis of tin(II) fluoride and crystal structure of Sn_4OF_6. *J. Chem. Soc., Dalton Trans.* **1994**, 2581–2583.
(21) Löber, M.; Geißenhöner, C. S.; Ströbele, M.; Romao, C. P.; Meyer, H. J. Synthesis, Structure and Electronic Properties of Three Tin Oxide Halides. *Eur. J. Inorg. Chem.* **2021**, *2021*, 283–288.
(22) von Schnering, H. G.; Nesper, R.; Pelshenke, H. $Sn_{21}Cl_{16}(OH)_{14}O_6$, the So-called Basic Tin(II) Chloride. *Z. Naturforsch.* **1981**, *36*, 1551–1560.
(23) Aurivilius, B. X-ray Studies of Lead Oxide Fluoride and Related Compounds. *Chem. Scripta* **1976**, *10*, 156–158.
(24) Zhang, H.; Zhang, M.; Pan, S.; Dong, X.; Yang, Z.; Hou, X.; Wang, Z.; Chang, K. B.; Poeppelmeier, K. R. $Pb_{17}O_8Cl_{18}$: A Promising IR Nonlinear Optical Material with Large Laser Damage Threshold Synthesized in an Open System. *J. Am. Chem. Soc.* **2015**, *137*, 8360–8363.
(25) Vincent, H.; Perrault, G. Crystal Structure of Synthetic Lead Oxychloride. *Bull. Soc. Francaise Mineral. Cristallogr.* **1971**, *94*, 323–331.
(26) Bondi, A. van der Waals Volumes and Radii. *J. Phys. Chem.* **1964**, *68*, 441–451.
(27) Beck, H. P.; Nau, H. Zur Kenntnis der Phasen $A_{2-2x}Sn_{5+x}Cl_{12}$ (A = K, In). *Z. anorg. allg. Chem.* **1988**, *558*, 193–200.
(28) Poulsen, F. R.; et al. Crystal Structure and Phase Transition of Cesium Trichlorostannate(II). *Acta Chem. Scand.* **1970**, *24*, 150–156.
(29) Shannon, R. D. Revised Effective Ionic Radii and Systematic Studies of Interatomic Distances in Halides and Chalcogenides. *Acta Crystallogr. A* **1976**, *32*, 751–767.
(30) Müller, U.; Mronga, N.; Schumacher, C.; Dehnicke, K. Die Kristallstrukturen von $PPh_4[SnCl_3]$ und $PPh_4[SnBr_3]$/ The Crystal Structures of $PPh_4[SnCl_3]$ and $PPh_4[SnBr_3]$. *Z. Naturforsch.* **1982**, *37*, 1122–1126.
(31) Ogden, J. S.; Ricks, M. J. Matrix Isolation Studies of Group IV Oxides. III. Infrared Spectra and Structures of SnO, Sn_2O_2, Sn_3O_3, and Sn_4O_4. *J. Chem. Phys.* **1970**, *53*, 896–903.
(32) Geurts, J.; Rau, S.; Richter, W.; Schmitte, F. J. SnO Films and Their Oxidation to SnO_2: Raman scattering, IR Reflectivity and X-ray Diffraction Studies. *Thin Solid Films* **1984**, *121*, 217–225.
(33) Becker, M.; Polity, A.; Klar, P. J.; Meyer, B. K. Synthesis of tin oxides SnO_{2-x} in the entire composition range (x = 0 to 1) by ion-beam sputter-deposition. *Phys. Status Solidi* **2015**, *9*, 326–330.
(34) Balgude, S. D.; Sethi, Y. A.; Kale, B. B.; Munirathnam, N. R.; Amalnerkar, D. P.; Adhyapak, P. V. Nanostructured Layered Sn_3O_4 for Hydrogen Production and Dye Degradation Under Sunlight. *RSC Adv.* **2016**, *6*, 95663–95669.
(35) Schrenk, C.; Köppe, R.; Schellenberg, I.; Pöttgen, R.; Schnepf, A. Synthesis of Tin(I) Bromide. A Novel Binary Halide for Synthetic Chemistry. *Z. Anorg. Allg. Chem.* **2009**, *635*, 1541–1548.
(36) Seko, A.; Togo, A.; Oba, F.; Tanaka, I. Structure and Stability of a Homologous Series of Tin Oxides. *Phys. Rev. Lett.* **2008**, *100*, No. 045702.
(37) Iliev, M.; Sinyukov, M.; Cardona, M. Resonant First- and Second-Order Raman Scattering in Gray Tin. *Phys. Rev. B* **1977**, *16*, 5350–5355.

https://doi.org/10.1021/acs.inorgchem.1c03763
Inorg. Chem. 2022, 61, 4018–4023